Agr. Nat. Resour. 56 (2022) 121–138

AGRICULTURE AND NATURAL RESOURCES

Journal homepage: http://anres.kasetsart.org

Research article

Novel, bioactive film based on methylcellulose incorporated with quercetin-loaded nanoparticles: Bifunctional antioxidant and ultraviolet-shielding properties

Kanthika Nantapreecha[a], Supoj Pratheepthinthong[b], Amporn Sane[a,c], Panuwat Suppakul[a,c,d,*]

[a] *Department of Packaging and Materials Technology, Faculty of Agro-Industry, Kasetsart University, Bangkok 10900, Thailand*

[b] *Thai Packaging Centre, Thailand Institute of Scientific and Technological Research, Bangkok 10900, Thailand*

[c] *Center for Advanced Studies in Nanotechnology and Its Applications in Chemical, Food and Agricultural Industries (CASNACFAI), Kasetsart University, Bangkok 10900, Thailand*

[d] *Center for Advanced Studies in Agriculture and Food (CASAF), Kasetsart University, Bangkok 10900, Thailand*

Article Info

Article history:
Received 25 August 2021
Revised 25 October 2021
Accepted 22 December 2021
Available online 25 February 2022

Keywords:
Antioxidant,
Bioactive film,
Biopolymer,
Quercetin,
UV-shielding

Abstract

A novel, bifunctional nanocomposite methylcellulose (MC) film was developed with antioxidant and ultraviolet (UV)-shielding properties. Quercetin (QC) nanoparticles (NPs) with an average size of approximately 60 nm were generated using a rapid expansion process. Quantification of the total phenolic content (TPC) was performed, followed by three assays—2,2-diphenyl-1-picrylhydrazyl (DPPH) radical scavenging, 2,2'-azino-bis (3-ethylbenzthiazoline-6-sulphonic acid) (ABTS) radical cation decolorization and ferric reducing antioxidant power (FRAP)—to investigate the antioxidant effectiveness of the QC-NPs. The QC-NPs had a TPC value of 1,619.59 µg gallic acid equivalents/mg and high antioxidant activities. The QC-impregnated MC films with all treatments (impregnated with ethanol (QC-EtOH)-, nanoparticles (QC-NPs) or water (QC-H_2O-MC) with concentrations of 0.1–0.5% w/w) were fabricated using the solution casting technique and characterized. The addition of QC into the MC films was substantiated using Fourier transform infrared spectroscopy. Impregnation of the QC-NPs into the MC film demonstrated that the QC-NPs augmented the antioxidant activities of QC and substantially improved the UV-shielding property of the MC film.

Introduction

The sensory attribute of agricultural and food products can be considered as a key element of their consumer acceptance and satisfaction that encourages purchase of the products. The oxidation of lipids as accelerated by ultraviolet light (UV) exposure is one of the crucial parameters impacting a loss in product quality and a decrease in shelf life, as the photo-oxidative and oxidative processes in food products

* Corresponding author.
E-mail address: panuwat.s@ku.ac.th (P. Suppakul)

https://doi.org/10.34044/j.anres.2021.56.1.12

result in the deterioration of lipids and proteins, leading to the nutritional and sensorial deteriorations of the products (Choe and Min, 2009). Consequently, shielding UV light exposure and retarding lipid oxidation are markedly pertinent to the food manufacturing sector.

In general, photo-oxidation and oxidation can be delayed by using UV-shielding materials and antioxidants, respectively (Lizundia et al., 2016). The addition of antioxidants to the food directly is not efficient, whereas an alternative means is an incorporation of bioactive agents that possess UV-shielding and antioxidant (AO) properties into biopackaging materials (Gómez-Estaca et al., 2014). Synthetic antioxidants have been famously adopted in the food industry. Nevertheless, the adoption of these antioxidants has been questioned because of their safety (Sanches-Silva et al., 2014). Consequently, natural antioxidants have gained more attention than synthetic antioxidants in past years (Sanches-Silva et al., 2014; Ganiari et al., 2017).

Quercetin (QC, 3,3′,4′,5,7-pentahydroxyl-flavoneis classified in the flavonol group and can be found in several fruits and vegetables (Materska, 2008). QC is well-known for its outstanding AO activity as it enables the eradication of reactive oxygen and nitrogen species to enhance the body's AO capacity by controlling levels of glutathione (GSH, Boots et al., 2008). In addition, it can chelate metal ions that initiates free radicals (Xu et al., 2019). Furthermore, QC has an antimicrobial (AM) property (Zheng et al., 2017), an anti-inflammatory property and an anticancer property in the breast, liver and colon (Bukhari, et al., 2008). Recently, QC has been incorporated in bilayer plastic films using the co-extrusion technique (Lu and Lu, 2018).

A limitation of QC is its poor water-solubility. A possible approach to solve this problem is nanotechnology. Nanoparticles (NPs) were conjoined with bioactive packaging to implicitly permit the utilization of lower dosages of bioactive substances in conjunction with a rise in surface area, an improvement in dissolution and a boost in bioactivity (Hannon et al., 2015). Many techniques have been applied to improve QC properties, such as high pressure homogenization, bead-milling, precipitation, supercritical antisolvent precipitation induced by the fast dissolution of a liquid solution of QC in supercritical carbon dioxide, solvent evaporation and encapsulation (Dehghan and Khoshkam, 2012; Maalik et al., 2014; Kumar et al., 2016). Nevertheless, some techniques have drawbacks. For example, the bioactive compounds are degraded because of chemical, shear stress or heat sensitivity. As an adaptable technique, the rapid expansion of sub- or supercritical solutions into liquid solvent (RESOLV) process involves the sub- or supercritical solution being directly expanded into a liquid receiving solution (typically aqueous in nature) that may or may not contain a stabilizing agent (Sane and Thies, 2005). This supercritical fluid technology creates stable, well-dispersed and uniform nanosuspensions at low temperature and uses less to none of the organic solvents that is plus for the environment (Kumari et al., 2010; Kakran et al., 2012; Hatahet et al., 2016). The advantages of the RESOLV process include producing smaller nanoparticles with narrow size distributions, nanoparticles that are readily dispersed in a liquid medium containing a small amount of dispersing agent and a nanosuspension is directly obtained from the process (Türk, 2009; Songtipya et al., 2016). However, there are still some limitations to the RESOLV process, such as the active compound needs to be dissolved in supercritical carbon dioxide, otherwise the addition of a suitable organic solvent is required to improve the solvent power of supercritical carbon dioxide.

Apart from safety, consumers are also concerned about the environment. As a promising biomaterial, cellulose is the most abundant organic renewable resource in the kingdom Plantae. It is a polysaccharide consisting of straight chains of several hundred to many thousands of (1−4)-β-D-glucopyranosyl units; as a cellulose derivative, methylcellulose (MC) has exclusively physical, chemical, colloidal and film-forming properties and accordingly, it has been used as edible packaging since the 1980s (Kester and Fennema, 1986). Methyl cellulose possesses good film-forming characteristics as the films are generally odorless, tasteless, flexible, transparent, resistant to fat and oil, water soluble, of moderate strength and exhibit moderate moisture and O_2 barrier properties (Bourtoom, 2008). For example, as a film-forming matrix, MC has been used for moisture blocking film by the incorporation of a fatty acid blend to enhance the shelf life of fresh eggs (Suppakul et al., 2010). Gasti et al. (2021) reported on biologically active and pH responsive smart films based on a chitosan/MC matrix integrated with *Phyllanthus reticulatus* ripened fruit anthocyanin to retard lipid oxidation and microbial inhibition and to monitor the freshness of fish fillets.

Park et al. (2020) envisaged that nanoscale manufacturing will be used as an innovative tool for the future development of smart food packaging systems. When biocomposite materials are entirely sourced from biobased constituents, desirable advantages such as biodegradability and biocompatibility are accentuated (Johnson et al., 2009). Lopez-Rubio et al. (2006) provided an extensive review and proposed a new grade of

special functional bioactive packaging materials. Numerous nanoparticle-related bioactive packaging films have been investigated. For example, Sonkaew et al. (2012) reported on the AO activities of cellulose-based films containing either curcumin NPs or ascobyl dipalmitate NPs. Saelo et al. (2016) reported on the AO and AM properties of cellulose-based films incorporating caffeic acid phenethyl ester NPs. De Moraes Crizel et al. (2018) reported on the AO effectiveness of olive pomace flour-impregnated chitosan films. Goudar et al. (2021) investigated the influence of zinc oxide nanoparticles (ZnO-NPs) on the physicochemical properties of a poly(vinyl alcohol) (PVOH)/*Spathodea campanulata* bud fluid matrix. However, the scientific findings are limited on the fabrication of QC into packaging films (Souza et al., 2015; Ezati and Rhim, 2021; Tavassoli et al., 2021). Therefore, the current work aimed: 1) to prepare QC-NPs using a rapid expansion of subcritical solutions into liquid solvents using the RESOLV approach; 2) to determine the AO activities of QC-NPs; and 3) to assess the AO activities and UV-shielding property of QC-NPs impregnated in cellulosic packaging films.

Materials and Methods

Materials

Quercetin (> 95% purity; CAS Number: 117-39-5) was obtained from Sigma-Aldrich (India). 2,2-Diphenyl-1-picrylhydrazyl or DPPH (CAS Number: 1898-66-4), Trolox (6-hydroxy-2,5,6,8-tetramethylchroman-2-carboxylic acid; CAS Number: 53188-07-1), Iron (III) chloride hexahydrate (CAS Number: 10025-77-1) and Folin-Ciocalteu phenol reagent (CAS Number: 12111-13-6) were purchased from Sigma-Aldrich (Germany), Sigma-Aldrich (Russia), Applichem (Germany) and Fluka (Switzerland), respectively. 3-tert-Butyl-4-hydroxyanisole or BHA (CAS Number: 25013-16-5) and 3,5-ditert-butyl-4-hydroxytoluene or BHT (CAS Number: 128-37-0) were supplied by Sigma-Aldrich (France) and Sigma-Aldrich (USA), consecutively. Pluronic F127 (CAS Number: 9003-11-6), 2,2′-Azobis(2-methylpropionamidine) dihydrochloride (CAS Number: 2997-92-4), and sodium acetate trihydrate (CAS Number: 6131-90-4) were purchased from Sigma-Aldrich (USA) and Sigma-Aldrich (Canada), respectively. Carbon dioxide (CO_2, ≥ 99.98% purity; CAS Number: 124-38-9) was obtained from Chattakorn Lab Center (Thailand). Ethanol (99.9% purity; (CAS Number: 64-17-5) was purchased from Merck (Germany). Food grade MC (METHOCEL™ A4C Premium) (methoxyl: 27.5–31.5%; viscosity: 320–480 cP; CAS Number: 9004-67-5) and poly(ethylene glycol) or PEG-400 (Carbowax) (molecular weight 380–420 g/mol; CAS Number: 25322-68-3) were supplied by Dow Chemical (USA) and Union Carbide (USA), respectively.

Preparation of quercetin nanoparticles

The RESOLV experiments were performed according to Chafer et al. (2004) and Sonkaew et al. (2012). The variable-volume view cell (48 mL) was charged with QC solution (16.1 g) prepared by dissolving QC in absolute ethanol at a concentration of 0.6% (weight per weight, w/w) and subcritical CO_2 (16.1 g). The QC solution in absolute ethanol was prepared prior to charging into the cell in order to accelerate the dissolution of active compound due to the solvent power of ethanol being higher than that of the ethanol-CO_2 mixture. Then, the mixture was pressurized to 173 bar, warmed to approximately 50°C and steadily stirred for approximately 1 hr or until a homogeneous solution was achieved, as the mixture turned to a transparent solution when observed using a borescope through the sapphire window of the view cell. Notably, the conditions of 173 bar and approximately 50°C were applied based on a preliminary study that had shown that the solution of 0.3% (w/w) in ethanol-CO_2 (1:1 w/w) mixture remained in one liquid phase for these conditions. Next, pure supercritical CO_2 was permitted to flow from the syringe pump, bypassing the high-pressure cell, and subsequently to expand across the nozzle (50 µm diameter) to set the steady-state conditions with a pre-expansion temperature (T_{pre}) and pressure (P_{pre}), upstream of the nozzle, of 80°C and 173 bar, respectively (Fig. 2). Then, the flow of pure CO_2 was quickly transferred to the view cell, indirectly pushing the subcritical solution out of the cell via a movable piston. The solution was dilated through the nozzle into 50 mL of 0.1 wt% pluronic F127, under ambient conditions, and a solution was obtained by immersing the nozzle 1 cm below the liquid surface. Probe ultrasonication was used with the intent of randomly distributing QC-NPs, because it generated greater productive energy output into the suspension. Pluronic F127, an ionic surfactant, was used to disperse and stabilize the QC-NPs in an aqueous solution.

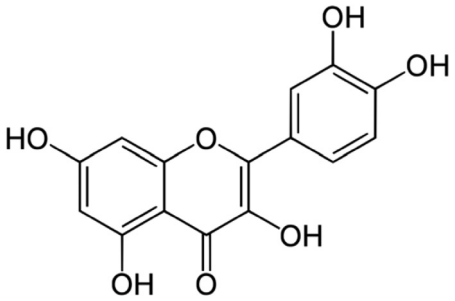

Fig. 1 Chemical structure of quercetin

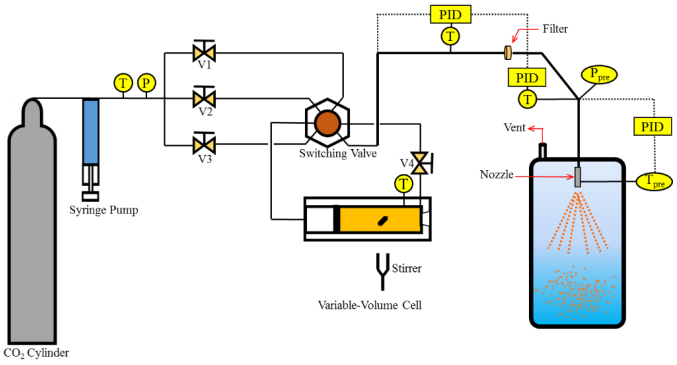

Fig. 2 Schematic of rapid expansion of sub- or supercritical solutions into liquid solventapparatus, where T = temperature; P = pressure; V1 = valve 1; V2 = valve 2; V3 = valve 3; V4 = valve 4; PID = proportional integral derivative;T_{pre} = pre-expansion temperature; P_{pre} = pre-expansion pressure

Quantification of quercetin nanoparticles

The protocol was slightly modified from Bukhari et al. (2008). A standard solution of QC in ethanol was provided by dissolving 5 mg of substance in 50 mL of 95% ethanol solution. The assay system used a UV-2450 UV-vis spectrophotometer (Shimadzu, Tokyo, Japan) at 200–700 nm for measuring the maximum wavelength (λ_{max}) of the compounds. To receive an absorbance standard curve of QC, serial dilutions of 1–10 µg/mL of QC in ethanol were analyzed. Two major absorption bands were found at 256 nm and 374 nm that were associated with the A and B rings, respectively. A maximum wavelength of 374 nm was used to predict the actual concentration. Absorbance was in the range 0.132–0.816 and the coefficient of determination (R^2) was 0.9959. Data were plotted in a straight line for the measurement of unknown samples in a nanosuspension.

Particle size distribution

The particle size and morphology of QC-NPs were investigated using two methods, namely transmission electron microscopy (TEM) and dynamic light scattering (DLS).

The TEM samples were processed in a transmission electron microscope (Tecnai 20 TWIN; Amsterdam, the Netherlands), by depositing approximately10 µL of the RESOLV suspension onto carbon coated or uncoated copper grids and dried at ambient temperature (Sonkaew et al., 2012). The particle sizes were analyzed using the Image-Pro Plus version 6.0 software (Media Cybernetics, Inc., Rockville, MD, USA).

For DLS, QC particles in aqueous suspension were characterized using a zetasizer Nano ZSP (Malvern Instruments, Malvern, UK) to compute the hydrodynamic diameter (d_h) of the QC particles (de Paz et al., 2015). The refractive indices of quercetin and distilled water used were 1.823 and 1.333, respectively. The d_h was computed from the translational diffusion coefficient (D) using the Malvern software package on the basis of Brownian motion theory and the Stokes-Einstein equation, as expressed in Equation 1:

$$d_h = \frac{kT}{3\pi\eta D} \quad (1)$$

where k is Boltzmann's constant, T the absolute temperature and η is the suspending medium viscosity, which was water at ambient conditions (1 atmosphere, 25°C). The viscosity of water under these conditions was 0.89 mPa.s).

Quercetin solution preparation

For the preparation of QC in ethanol (QC-EtOH), BHA, and BHT 10 mg of each substance was separately dissolved in 100 mL of 40% ethanol and directly used as the stock solution of the substance.

The stock solution of QC in water (QC-H_2O) was prepared in accordance with Sonkaew et al. (2012), by adding 30 mg of QC into 100 mL of distilled water and placing in an ultrasonic water bath (Crest Ultrasonics Corporation; Sunrise, FL, USA) with a sweep frequency of 45 kHz and switch-on duration of 100% (continuous operation) for 10 min. Then, the suspension was centrifuged at 1,000 revolutions per minute for 10 min and the supernatant was applied as stock solution of QC-H_2O. The concentrations of all stock solutions were measured using ultraviolet-vis spectrophotometry.

Total phenolic content and antioxidant activities determination

Total phenolic content assay

The total phenolic content (TPC) was evaluated using the Folin-Ciocalteu method based on Song et al. (2010) with slightly modification. Briefly, 0.50 mL of active substances was blended with 2.5 mL of Folin-Ciocalteu reagent (1:10 volume per volume distilled water). An amount of 2 mL 7.5% w/v sodium carbonate was incorporated into the blend and vortexed. The blend was left in the dark under ambient conditions for 30 min to produce a blue-colored mixture. The solution was quantified at an absorbance of 765 nm and a calibration plot was generated using gallic acid at different concentrations. The results were presented as micrograms of gallic acid equivalent per milligram of solid sample (µg GAE/mg).

2,2-Diphenyl-1-picrylhydrazyl radical scavenging assay

The DPPH radical scavenging activity of selected substances was assessed in accordance with Sonkaew et al. (2012) with some modification. Separately, 1 mL of each diluted sample (BHA, BHT, QC-EtOH, QC-NPs or QC-H_2O) in 0.1 wt % pluronic F127 solutionwas added to 0.5 mL of 0.4 mM DPPH radical in 0.1 wt % pluronic F127 solution at different concentrations. The solutions were vortexed homogeneously and incubated for 30 min in the dark at room temperature. All experiments replicated three times. The absorbance of the solution was measured at 519 nm. The percentage of free radical scavenging was determined using Equation 2. The sample dosage producing 50% radical scavenging activity (EC_{50}) was computed from the curve of DPPH scavenging percentage against its dosage.

$$\text{DPPH radical scavenging (\%)} = \left[\frac{\text{absorbance of sample}}{\text{absorbance of control}}\right] \times 100 \quad (2)$$

2,2'-Azino-bis (3-ethylbenzthiazoline-6-sulphonic acid) radical cation scavenging assay

ABTS forms a comparatively stabilized free radical, which decolorizes in its nonradical form. Assay of ABTS radical cation scavenging activity via spectrophotometry was measured using a modification of Dueñas et al. (2010). In this protocol, ABTS radical cations were created by reacting 2 mM ABTS in H_2O with 2.45 mM potassium persulfate ($K_2S_2O_8$), and then keeping the solution in the dark under ambient conditions for 16 h. The ABTS radical cation solution was diluted to yield an absorbance at 734 nm in 0.1 wt % pluronic F127 solution. Then, 600 µL of ABTS radical cation solution was added with 600 µL of each sample solution (BHA, BHT, QC-EtOH, QC-NPs or QC-H_2O) in 0.1 wt % pluronic F127 solution at various dosages. The absorbance was logged for 30 min after blending, and the percentage of radical scavenging was expressed for each concentration corresponding to a blank solution containing no scavenger (Equation 3):

$$\text{ABTS radical scavenging (\%)} = \left[\frac{\text{absorbance of sample}}{\text{absorbance of control}}\right] \times 100 \quad (3)$$

The sample dosage producing 50% radical scavenging activity (EC_{50}) was determined from the curve of the ABTS radical cation scavenging percentage against its dosage.

Ferric reducing antioxidant power assay

Ferric reducing antioxidant power assay was carried out with minor modifications to the methods of Thaipong et al. (2006) and Lee et al. (2016). The protocol was based on the reduction of a ferric 2,4,6-tripyridyl-s-triazine complex (Fe^{3+}-TPTZ) to the ferrous form (Fe^{2+}-TPTZ). The stock solutions comprised: 300 mM acetate buffer of pH 3.6; 10 mM 2,4,6-tripyridyl-s-triazine (TPTZ) solution in 40 mM HCl; and 20 mM $FeCl_3.6H_2O$ solution. Fresh working solution was arranged by blending acetate buffer, TPTZ solution and $FeCl_3 \cdot 6H_2O$ solution in a 10:1:1 ratio, and then permitting the reaction at 37 °C prior to usage. BHA, BHT, QC-EtOH, QC-NPs and QC-H_2O (with a volume of 150 µL at a concentration of 25 µg/mL) were filled to 3,000 µL of fresh working solution and permitted to react for 30 min in the dark. A rise in absorbance at 593 nm was monitored. Series solutions of Trolox showed a straight-line calibration graph with linearity in the range 25–800 µM/mL. These reductions were calculated as Trolox equivalents in micromolars per milliliter (TE µM/mL).

Bioactive-incorporated methylcellulose film preparation

Cellulose ether solution was prepared consistent with Sonkaew et al. (2012) and Saelo et al. (2016). Selected substance solutions (BHA, BHT, QC-EtOH, QC-NPs or QC-H_2O) were then filled with cellulose ether solution to acquire various concentrations (0.1 wt%, 0.2 wt%, 0.3 wt%, 0.4 wt% and 0.5 wt%). The solutions were degassed in an ultrasonic water bath (model 275D; Crest Ultrasonics; Trenton NJ, USA) for 4 min. Bioactive films were prepared according to Sonkaew et al. (2012) and Saelo et al. (2016).

Film characterization

Film thickness measurement

A digital micrometer (model 7326; Mitutoyo Manufacturing; Tokyo, Japan) was used to measure the thickness of each film.

Film opacity measurement using ultraviolet-vis spectrophotometry

UV-vis spectrophotometry was carried out according to the procedure of Saelo et al. (2016) with minor modification. Square films (3.0 cm × 3.0 cm) were mounted directly onto the spectrophotometer test cell and their absorbance spectra were acquired using a UV-2450 UV-vis spectrophotometer (Shimadzu Corporation; Tokyo, Japan). An empty test cell was used as the reference. The degree of opacity (T value) of each film at λ_{max} was expressed using Equation 4:

$$T = \frac{\text{Abs of sample at } \lambda\text{max}}{x} \quad (4)$$

where Abs of sample at λ_{max} is the value of absorbance at the maximum wavelength and x is the film thickness in millimeters. A lower value of T signifies greater transparency and less opacity, while a higher value indicates the opposites. All treatments were replicated five times.

Morphological characterization using scanning electron microscopy

A 1450VP scanning electron microscope (LEO; Cambridge, UK) was used to investigate the morphology of NPs and films, conforming to Sonkaew et al. (2012) and Saelo et al. (2016).

Functional group analysis using Fourier transform infrared spectroscopy

The FTIR spectra of the MC and the FTIR spectra of MC films impregnated with QC-EtOH, QC-NPs and QC-H_2O were taken using a Bruker Tensor 27 FTIR spectrometer (Bruker; Karlsruhe, Germany) consistent with Sonkaew et al. (2012) and Saelo et al. (2016). In the attenuated total reflectance (ATR) mode, the measurement area was adjusted to an aperture of 150 µm × 150 µm. The FTIR spectra were used to examine the corporality of functional groups of QC in the different MC films.

Determination of total phenolic content and antioxidant activities of the films

Total phenolic content assay

The TPC was tested as reported in the previous section. A 6 cm^2 sample of bioactive film was dissolved in 6 mL of the solution containing 0.1 wt % pluronic F127. Then, 0.50 mL of film extract was blended with 2.5 mL of 0.2 M Folin-Ciocalteu reagent and 2 mL of 7.5% weight per volume (w/v) Na_2CO_3 and permitted to react for 30 min in the dark. All treatments were replicated three times.

2,2-Diphenyl-1-picrylhydrazyl radical scavenging assay

Free radical scavenging activity was examined as described by Siripatrawan and Harte (2010) with slight modifications. A 6 cm^2 sample of bioactive film was dissolved in 6 mL of solution containing 0.1 wt % pluronic F127. Then, 1 mL of film extract solution was added with 0.5 mL of DPPH radical (0.4 mM) in 40% ethanol and permitted to react for 30 min in the dark. All treatments were replicated three times.

ABTS radical cation scavenging assay

ABTS assay was performed as reported in the previous section. A 6 cm^2 sample of AO film was dissolved in 6 mL of solution containing 0.1 wt% pluronic F127. Then, 1 mL of film extract solution was mixed with 2 mM of ABTS radical cation solution in 0.1 wt% pluronic F127 and permitted to react for 30 min in the dark. All treatments were replicated three times.

Ferric reducing antioxidant power assay

FRAP assay was determined as expressed in the previous section. A 6 cm^2 sample of bioactive film was dissolved in 6 mL of solution containing 0.1 wt% pluronic F127. Then, 150 µL of film extract solution was mixed with 3 mL of ferric reagent and permitted to react for 30 min in the dark. All experiments replicated three times.

In all experiment, the treatments were assigned following a completely randomized design. All treatments were carried out in three replicates and five replicates for the antioxidant assays and degree of opacity testing, respectively.

Data analysis

All data were analyzed using one-way analysis of variance using the SPSS 16.0 for Windows software (SPSS Inc.; Chicago, IL, USA). Then means were compared using Duncan's multiple range test. The tests were considered significant at $p < 0.05$.

Results and Discussion

Morphology of quercetin nanoparticles

During expansion of the subcritical solution into the receiving liquid, in which ethanol was used as a solvent, the solute precipitated QC as a solid, while the CO_2 expanded to form a low-pressure gas surrounded by the liquid receiving solution. The solid and liquid phases came into contact at the solid-liquid interface. Clearly, this phenomenon was a wetting process. Using the addition of pluronic F127 as a stabilizing agent to modify the wetting characteristics of the receiving solution, the dispersibility of the QC-NPs formed in RESOLV could be influenced and even perhaps controlled. The verified quantity of QC-NPs in aqueous suspension quantified using UV-vis spectrophotometry was 2.68 ± 0.60 mg/mL. The primary QC-NPs were manifestly individual yellow particles in aqueous suspension (Fig. 3). However, after a long period of storage (> 6 mth), it was evident that they tended to agglomerate and precipitate. Fortunately, probe ultrasonication was effective at resuspending and dispersing the QC-NP agglomerates, as was also reported by Jiang et al. (2009) who revealed that bath ultrasonication was worse than probe ultrasonication in dissipating TiO_2 agglomerates, using sodium pyrophosphate as a stabilizing agent.

The TEM results showed that the QC-NPs produced were spherical, well-dispersed and less than 150 nm in diameter. The average diameter ($\bar{d}_p$) of the QC-NPs was 57 nm with a range of 17–129 nm (Fig. 3 and Table 1). Multiple TEM images at the same magnification (10,000×) were used to measure all particle sizes. Montes et al. (2015) produced QC-NPs using a supercritical antisolvent precipitation technique (250 bar, 65°C) and produced the smallest nanoparticles size of 150 nm, while Fernández-Ponce et al. (2014) also applied a supercritical antisolvent precipitation technique (100 bar, 35°C), producing QC-NPs with a size of 180 nm. Compared with other methods, the average size produced by the RESOLV technique was smaller perhaps because of the rapid expansion of the subcritical solution of QC directly into the receiving solution containing the dispersant, so that the initially formed nanoparticles were readily dispersed in the liquid and particle growth via the coagulation process was reduced (Sane and Thies, 2005). DLS analysis revealed that the polydispersity index (PDI) of QC-NPs was 0.415, indicating the broadness of the size distribution (Bhattacharjee, 2016). The hydrodynamic diameter (d_h) range of the nanosuspension was 295–955 nm, with an average size of 489 nm (Fig. 4 and Table 1).

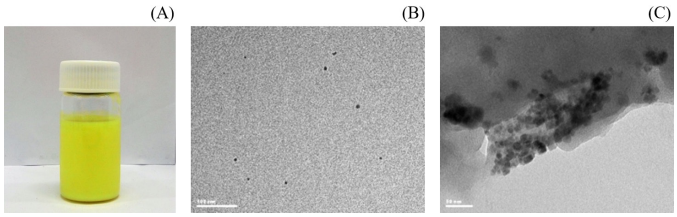

Fig. 3 (A) Aqueous suspension of quercetin nanoparticles (QC-NPs); (B, C) Transmission electron microscopy images of QC-NPs on a copper grid obtained from rapid expansion of sub- or supercritical solutions into liquid solvent technique at magnifications of 10,000× and 20,000×, respectively

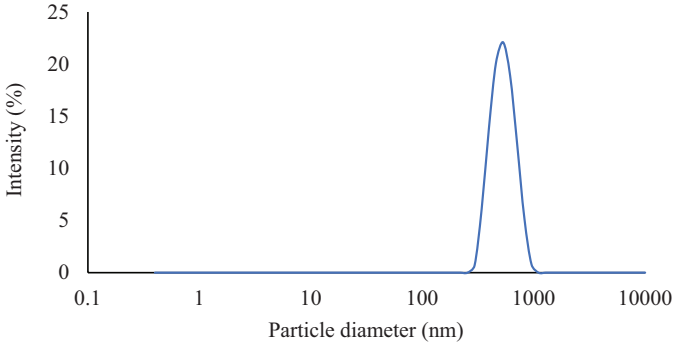

Fig. 4 Particle size distribution of quercetin nanoparticles

Table 1 Particle sizes obtained from dynamic light scattering (DLS) and transmission electron microscopy (TEM) measurements of quercetin nanoparticles (QC-NPs) prepared using rapid expansion of sub- or supercritical solutions into liquid solvent of 0.6 wt% solution with pre-expansion temperature (T_{pre}) and pressure (P_{pre}) of 80°C and 173 bar, respectively, into aqueous receiving solution containing 0.1 wt% pluronic F127

Antioxidant	DLS		TEM	
	d_h range (nm)	$\bar{d}_h$ (nm)	d_p range (nm)	$\bar{d}_p$ (nm)
QC-NPs	295–955	489	17–129	57

d_h = hydrodynamic diameter; d_p = particle diameter

There were large differences in particle sizes due to differences between the TEM and DLS methods. TEM is a direct technique that measures the maximum diameter and shape of individual nanoparticles, whereas DLS is a relative technique that measures the nanosuspension size from time-dependent fluctuations of scattered coherent light. Therefore, DLS cannot be used to differentiate between individual particles and agglomerates (Pabisch et al., 2012). Agglomerated particles were detected as a single particle, resulting in an overall larger particle size. In addition, there is a hydration layer around the particle surface that makes the particle size larger (Fissan et al., 2014). Thus, the agglomeration of QC-NPs was confirmed based on the TEM image (Fig. 3C).

Total phenolic content and antioxidant activities

Total phenolic content

As an indication of AO capacity, the highest TPC of the QC-NPs was 1,619.59 µg GAE/mg, followed by QC-EtOH (1,121.59 µg GAE/mg), QC-H_2O (749.69 µg GAE/mg) and BHT (407.13 µg GAE/mg) and BHA (347.59 µg GAE/mg), as shown in Table 2. The TPC for the QC-NPs was significantly higher than that of 426.74 µg GAE/mg for caffeic acid phenethyl ester nanoparticles (CAPE-NPs) (Saelo et al., 2016). This analysis was based on a reduction in the ability of the Mo^{6+} ion/AO capacity due to either the hydrogen-donating or electron-donating nature of polyphenol for scavenging free radicals, resulting in comparatively stable phenoxyl radicals (neutral or cationic molecules, respectively), which are maintained by delocalization of unpaired electrons around the aromatic ring, designated as radical resonance stabilization (Singleton and Rossi, 1965; Sánchez-Rangel et al., 2013).

2,2-Diphenyl-1-picrylhydrazyl radical scavenging capacity

The free radical scavenging capacities of the investigated substances (QC-EtOH, QC-NPs and QC-H_2O) were compared to those of BHA and BHT using DPPH radical scavenging assay. There was a highly significant difference among the mean DPPH radical scavenging values. Table 2 shows that the EC_{50} values of BHA and BHT were 10.35 µg/mL and 16.53 µg/mL, respectively. The EC_{50} values for the QC solutions of QC-NPs, QC-EtOH and QC-H_2O were 4.92 µg/mL, 4.97 µg/mL and 21.10 µg/mL, respectively. The EC_{50} value for QC-NPs was higher than the 2.93 µg/mL for curcumin nanoparticles (Ccm-NPs) (Sonkaew et al., 2012), and significantly lower than for ascorbyl dipalmitate nanoparticles at 76.32 µg/mL (Sonkaew et al., 2012) and for CAPE-NPs at 92.69 µg/mL (Saelo et al., 2016). A lower EC_{50} value signifies greater DPPH free radical scavenging effectiveness, and vice versa. The current results implied that QC-NPs and QC-EtOH were substantially better than BHA, BHT and QC-H_2O at radical scavenging, because the QC-NPs have a smaller particle size that increases the particle distribution, surface area and area of interaction, while these, in turn, enhance their free radical scavenging capacity. This result was consistent with other studies (Wu et al., 2008; Saelo et al., 2016). The free radical scavenging capacity of QC-H_2O decreased with increasing polarity as the higher polarity solvent induced stronger intermolecular interaction due to hydrogen bonding between the solvent and QC, leading to a substantial change in the H-atom donor activities of the phenolic compounds (Pinelo et al., 2004). In addition, Zheng et al. (2017) explained the AO capacity of QC by an intramolecular interaction in association with enthalpy between the oxygen and hydrogen in the hydroxyl group. QC-H_2O had higher enthalpy than QC-EtOH, indicating that the bond of OH groups in water were stronger than for the OH groups in ethanol. Consequently, QC-EtOH reacted more readily with free radicals than did QC-H_2O.

Table 2 Total phenolic content and antioxidant activities of 3-tert-Butyl-4-hydroxyanisole (BHA), 3,5-ditert-butyl-4-hydroxytoluene (BHT), quercetin (QC)-EtOH, QC-nanoparticles (NPs) and QC-H_2O

Antioxidant	TPC (µg GAE/mg)	DPPH scavenging; EC_{50} (µg/mL)	ABTS scavenging; EC_{50} (µg/mL)	FRAP (TE µM/mL)
BHA	347.59±15.98^{d}	10.35±2.02^{b}	3.50±0.45^{b}	127.87±4.44^{d}
BHT	407.13±39.10^{d}	16.53±1.29^{c}	3.59±0.40^{b}	37.24±4.92^{e}
QC-EtOH	1,121.59±3.17^{b}	4.97±0.80^{a}	2.10±0.08^{a}	258.51±6.74^{b}
QC-NPs	1,619.59±130.57^{a}	4.92±0.13^{a}	1.97±0.08^{a}	289.78±16.59^{a}
QC-H_2O	749.69±104.61^{c}	21.10±1.22^{d}	3.54±0.99^{b}	155.17±7.30^{c}

TPC = total phenolic content; DPPH = 2,2-diphenyl-1-picrylhydrazyl; ABTS = 2,2'-azino-bis (3-ethylbenzthiazoline-6-sulphonic acid); FRAP = ferric reducing antioxidant power; GAE = gallic acid equivalent; EC_{50} = 50% of radical scavenging activity; TE = Trolox equivalents
Values (mean ± SD) within the same column superscripted with different lowercase letters are significantly ($p < 0.05$) different.

DPPH in unstabilized form receives either an electron or hydrogen atom from QC through the SPLET mechanism (Foti et al., 2011). Based on the reduction of DPPH in QC, formation of the non-radical form DPPH-H occurred, where a B ring of QC contributed to free radical scavenging due to 1,2 dihydroxybenzene, known as catechol (Goupy et al., 2003). The incorporation of QC into the DPPH solution resulted in an expeditious decrease in the optical density at 519 nm. The scavenging capacity of QC was indicated by the degree of discoloration, between a dark purple colored solution of DPPH and a light-yellow colored solution of diphenyl-picryl hydrazine, where the extent of the reaction is dependent upon the hydrogen-donating or electron-donating ability of the antioxidants (Dehghan and Khoshkam, 2012).

2,2'-Azino-bis (3-ethylbenzthiazoline-6-sulphonic acid) radical cation scavenging capacity

ABTS radical cation scavenging capacity is shown in Table 2. The average ABTS radical cation scavenging values were highly significantly ($p < 0.01$) different in a similar fashion to the average DPPH radical scavenging values. This finding indicated that the QC-NPs had the greatest ABTS radical cation scavenging activity with an EC_{50} value of 1.97 µg/mL, followed by QC-EtOH (2.10 µg/mL), BHA (3.50 µg/mL), QC-H_2O (3.54 µg/mL) and BHT (3.59 µg/mL). The EC_{50} values for the QC-NPs were significantly lower than those of 51.34 µg/mL and 355.40 µg/mL for Ccm-NPs and ascorbyl dipalmitate (ADP)-NPs, respectively (Sonkaew et al., 2012). The ABTS radical cation was more reactive than the DPPH radical. A blue-green ABTS radical cation resulted from ABTS oxidation using potassium persulfate. Fading of the blue-green ABTS radical cation mixture has been used to assess the AO activity of individual substances. The ABTS radical cation is bleached by QC functional groups via the H-atom and the electron transfer mechanism, in the same manner as the DPPH reaction (Gordon, 1990; Alam et al., 2013).

Ferric reducing antioxidant power value

There was a highly significant ($p < 0.01$) difference among the average FRAP values, as tabulated in Table 2. The QC-NP solution had the highest FRAP value of 289.78 µM/mL, followed by QC-EtOH (258.51 µM/mL), QC-H_2O (155.17 µM/mL), BHA (127.87 µM/mL) and BHT (37.24 µM/mL). The FRAP values for the QC-NPs was significantly higher than that of 56.88 µM/mL for Ccm-NPs (Sonkaew et al., 2012) and significantly lower than that of 741.46 µM/mL for CAPE-NPs (Saelo et al., 2016).

It was evident that the AO capacity of QC relied strictly on the existence of phenolic functional groups, as indicated by the TPC. It has since been shown that phenolic hydrogens may be engaged in the mechanism of formation of the phenoxy radical. During the FRAP test, the existence of reductants in the tested samples reduced the Fe^{3+}-TPTZ complex to the ferrous form (Fe^{2+}). Gordon (1990) stated that the AO action of reduction is based on breakage of the radical chain by donation of a hydrogen atom. Additionally, the FRAP test produces information on the total AO potential in cells in a comparatively short time, without having to perform more lengthy tests for each individual AO (Griffin and Bhagooli, 2004). This finding strongly supports the adoption of the rapid expansion process to fit QC-NPs with a substantially favorable impact on the AO effectiveness of QC perhaps due to the short processing time and the absence of light and oxygen in the rapid expansion process, leading to minimization of undesirable oxidation reactions (Songtipya and Sane, 2013). Additionally, NPs via the RESOLV process could permit the utilization of lower dosages of bioactive substances, along with a rise in the surface area and an improvement in dissolution, resulting in an increase in their bioactivity.

Quercetin nanoparticles incorporated with methylcellulose film characteristics

Film thicknesses were in the range 45–55 µm but there were no significant differences among the samples. The appearance of the MC film and selected QC-EtOH-Mc film, QC-NPs-MC film and QC-H2O-MC film at 0.5 wt% are shown in Fig. 5. There was relative matching between PEG400 and MC in relation to the inclination for polar and hydrogen bonding interactions. They were subservient to the extended affinity, lessening the ability of PEG400 to lift effortlessly on the film surface, which, in turn, led to minimizing film embrittlement during long-term storage (Kitak et al., 2015).

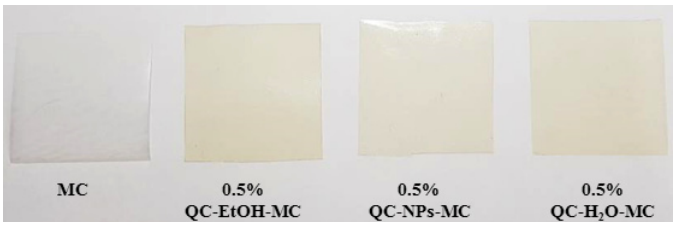

Fig. 5 Appearance of methylcellulose (MC) film and quercetin (QC)-EtOH-MC film, QC-nanoparticles-MC film and QC-H_2O-MC film at 0.5 wt%

Light transmittance

The UV-visible spectra of bioactive films are illustrated in Fig. 6A. Although sufficient UV protection was provided using only either QC-EtOH or QC-H_2O in the MC film, the QC-NPs-MC films with a concentration higher than 0.5 wt% could be superior regarding their UV shielding and antioxidant properties. The incorporation of QC-NPs into MC-based films affected optically transparency, with the transmittance depending on QC-NPs concentrations, namely, at 540–560 nm 370 nm and 300 nm being 86.46–88.93%, 3.38–68.38% and 7.54–47.02%, respectively. In the UV region, the transmittance values decreased with increasing QC concentrations, as presented in Table 3. The QC-NPs-MC films with 0.5 wt % incorporated had the highest UV-shielding property being able to absorb UV by reducing the transmittance value from 69.82% to 7.54% in the UV-B light range (280–315 nm) and reducing from 81.01% to 3.38% in the UV-A light range (315–400 nm) compared with the control MC film. These transparent QC-NPs-incorporated methylcellulose films had superior UV-shielding properties compared to other studies (Ahmed and Ikram, 2016; Lizundia et al., 2016; de Moraes Crizel et al., 2018; Hu et al., 2019; Shankar and Rhim, 2019). UV light is one of major deterioration factors affecting food quality via trigger oxidation and discoloration in meat products (Bekbölet, 1990). The ability to absorb UV light is termed band-gap absorption (Lizundia et al., 2016). The higher the band gap energy, the more UV light is absorbed. The band gap energy of QC was 3.98 eV, corresponding to the wavelength of 311 nm (Afia et al., 2016). Since the photon energies of UV-A and UV-B are 3.10–3.94 eV and 3.94–4.43 eV, respectively (Afia et al., 2016), QC could possibly absorb both UV-A and UV-B. Vilera et al. (2017) reported that phenolic compounds could absorb UV light due to their benzene rings.

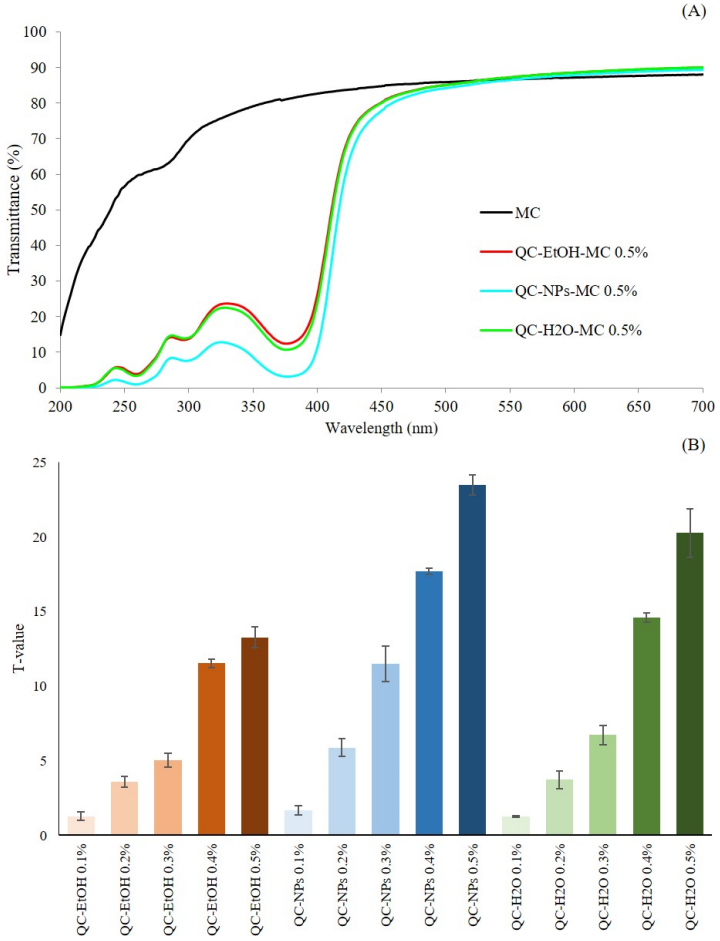

Fig. 6 Ultraviolet-vis transmittance spectra of: (A) 0.5 wt% quercetin (QC)-EtOH-MC, QC-nanoparticles (NPs)-MC and QC-H_2O-MC films in range 200–700 nm; (B) degree of opacity (*T* value) at 374 nm of QC-EtOH-MC, QC-NPs-MC and QC-H_2O-MC films at 0.1, 0.2, 0.3, 0.4 and 0.5 wt%, where error bars indicate ± SD

Table 3 Percentage transmittance of methylcellulose films containing quercetin (QC)-EtOH, QC-nanoparticles (NPs) and QC-H_2O at different concentrations

Antioxidant	Concentration (% weight per weight)	Wavelength		
		300 nm	370 nm	540–560 nm
–	–	69.82	81.01	86.62
QC-EtOH	0.10	49.34	73.80	88.39
	0.20	36.99	56.32	87.88
	0.30	25.16	37.08	87.59
	0.40	18.61	22.40	87.20
	0.50	13.70	12.93	87.37
QC-NPs	0.10	47.02	68.38	88.93
	0.20	28.21	36.31	87.83
	0.30	14.80	21.01	87.29
	0.40	10.68	6.80	87.05
	0.50	7.54	3.38	86.46
QC-H_2O	0.10	48.68	72.29	88.46
	0.20	33.89	53.05	87.82
	0.30	23.62	33.57	87.20
	0.40	18.17	19.40	87.53
	0.50	14.01	11.20	87.30

In addition, based on UV-visible spectroscopy, the interaction (absorption) of electromagnetic radiant with matter (such as QC-NPs) involves with the quantization of energy. The absorption of energy causes an atom or molecule to go from an initial energy state (ground state) to another higher energy state (excited state). The energy states are said to be quantized because there are only certain values that are possible—there is not a continuous spread of energy level available (Pungor, 1995). The absorption of UV radiation corresponds to the excitation of an outer electron that in turn involves electronic transition (ET), involving $\pi \rightarrow \pi^*$ transition energy of QC with a value of 352.7 nm (Andrade-Filho et al., 2009). Furthermore, QC will absorb harmful UV radiation and emit harmless radiation of a longer wavelength and lower energy, which is dissipated throughout the polymeric MC matrix via the mechanism of keto-enol tautomerism (Sisa et al., 2010).

Fig. 6B shows the *T* values of films, with QC λ_{max} at 374 nm. There was a significant reduction in the transparency of the QC-NPs−MC films compared to the control MC film, although it was only slight compared to the blank and was in the acceptable range for transparent edible films, as previously presented in Fig. 5.

Low-voltage scanning electron micrography

Fig. 7 illustrates the low-voltage scanning electron micrographs (LVSEM) of different types of QC solutions (at 0.5 wt%) in cellulose-based films at magnifications of 5,000× and 10,000×. The MC film incorporated with 0.5 wt% QC-EtOH had particle sizes in the range 100–2,000 nm on the surface of the film, akin to the 0.5 wt% QC-NP-impregnated MC film (50–200 nm). However, the particle size in the QC-NPs film were mostly smaller than that in QC-EtOH film and some particles in the QC-NPs film recrystallized to form a needle-like shape. The MC film impregnated with 0.5 wt% QC-H_2O had needle-shaped particles of a with larger size (1,000–2,000 nm).

The different shapes of the QC particles on the film surface could be explained Hatahet et al. (2016) who concluded that the different shapes of nanoparticles originated from particle agglomeration during the drying process, since the nanoparticles are thermodynamically unstable due to their large surface area and high surface energy. In addition, the spherical and needle-like shapes corresponded to QC structures in the amorphous and crystalline phases, respectively. Based on thermodynamic stabilization, QC-NPs tended to transform a spherical shape into a needle-like shape in order to minimize the surface energy (Fernández-Ponce et al., 2014).

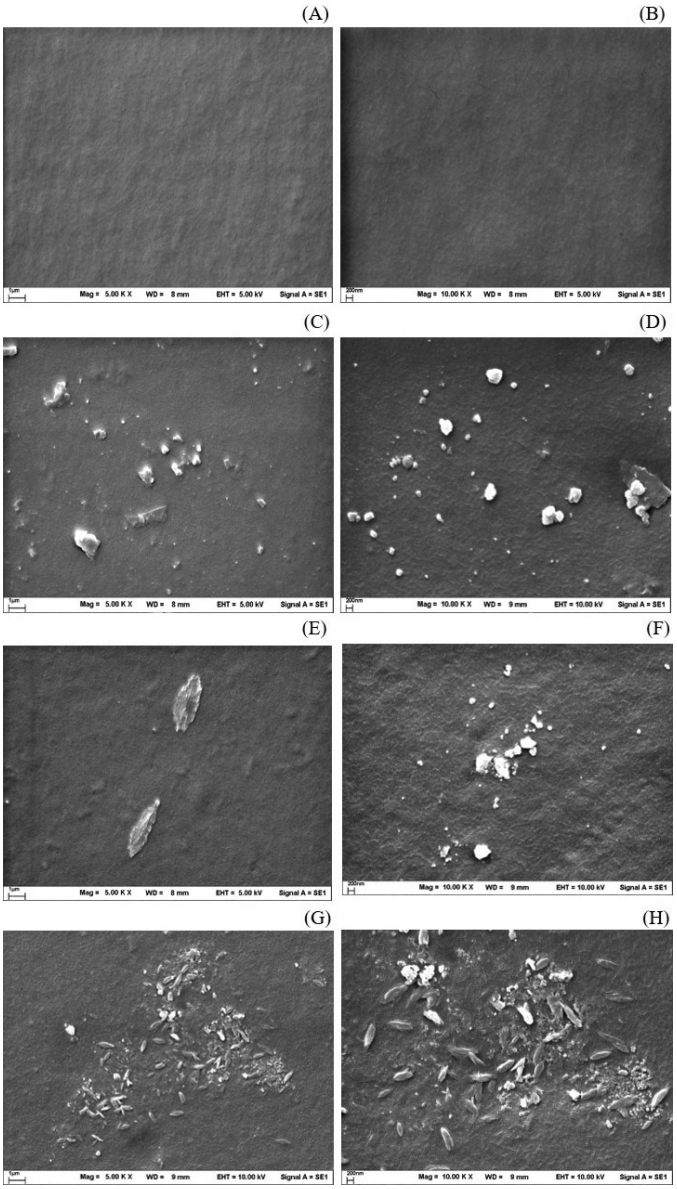

Fig. 7 Low-voltage scanning electron micrographs of various types of: (A, B) methylcellulose (MC) film; (C, D) 0.5 wt% quercetin (QC)-EtOH-MC film; (E, F) 0.5 wt% QC-H_2O-MC film; (G, H) 0.5 wt% QC-nanoparticles-MC film, at magnifications of 5,000× for A, C, E and G and at 10,000× for B, D, F and H

Functional groups

The functional groups of MC were investigated using FTIR spectroscopy as depicted in Fig. 8. The spectrum within the region 3800–3000 cm^{-1} was attributed to the stretching of O−H at 3450 cm^{-1}. The MC film had an absorption band associated with $–CH_3$ stretching in the anhydroglucose unit at 2962 cm^{-1}, $−CH_2−$ stretching in the anhydroglucose unit at 2893 cm^{-1}, C=O carbonyl stretching in the anhydroglucose unit of the cellulose at 1637 cm^{-1}, C−OH in-plane bending at 1454 cm^{-1}, $−CH_3$ symmetric bending at 1371 cm^{-1}, C−O stretching from the asymmetric oxygen bridge at 1163 cm^{-1}, C−O−C stretching at 1458, 1057 and 945 cm^{-1} and ring stretching at 891 cm^{-1}. These results were consistent with those reported by Viera et al. (2007); Khan et al. (2010); Rimdusit et al. (2012); and Tavera-Quiroz et al. (2012).

The chemical structure of QC is illustrated in Fig. 1. Based on the FTIR spectrum of QC, the band obtained at 3385 cm^{-1} was attributed to −OH stretching of a peak for the phenolic group. The strong and sharp peaks at 1657, 1243 and 1161 cm^{-1} were assigned to C=O (carbonyl group), C=C (benzene ring), and C−O (functional group of ester) stretching, respectively in accordance with Dehghan and Khoshkam (2012); Fraile et al. (2014) and Ravichandran et al. (2014), respectively. In addition, the characteristic peaks of QC were assigned to benzene ring stretching at 1562 and 1512 cm^{-1} (Cornard et al., 1997).

O−H stretching was observed at 3448.7 cm^{-1} for all film samples indicating there was no effect on film composition in this band. Nevertheless, the band symmetry was markedly distorted, as shown in Fig. 9. Band symmetry distortion (BSD) is the best designative behavior of binary systems and unveils the shift of hydrogen bond dynamism between their components (Cangelosi and Shaw, 1983). To obtain BSD, $\Delta_{1/2}$ can be determined at the spectral bandwidth as the span of the band of light at half the peak maximum (Vinogradov and Linnell, 1971). The impregnation of QC-EtOH, QC-H_2O and QC-NPs into MC films led to BSDs of 86.80 cm^{-1}, 84.96 cm^{-1} and 82.94 cm^{-1}, consecutively, compared to 92.59 cm^{-1} for the MC film BSD. Therefore, the variances in BSD among the MC film and QC-EtOH-Mc film, QC-H_2O-MC film

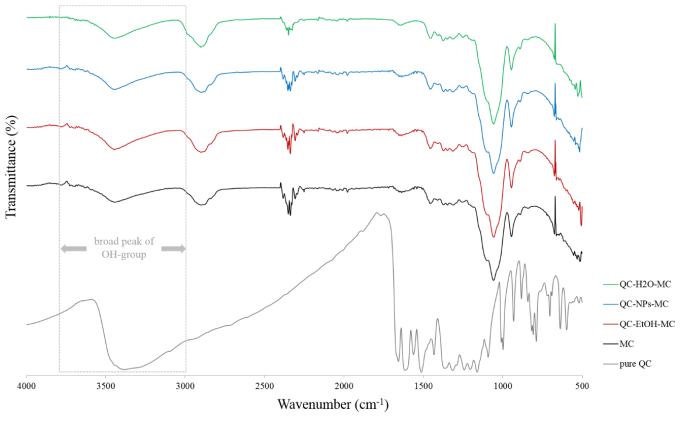

Fig. 8 Fourier transform infrared spectroscopy spectra of methylcellulose (MC) and 0.5 wt% quercetin (QC)-EtOH-MC film, QC-nanoparticles-MC film and QC-H_2O-MC film

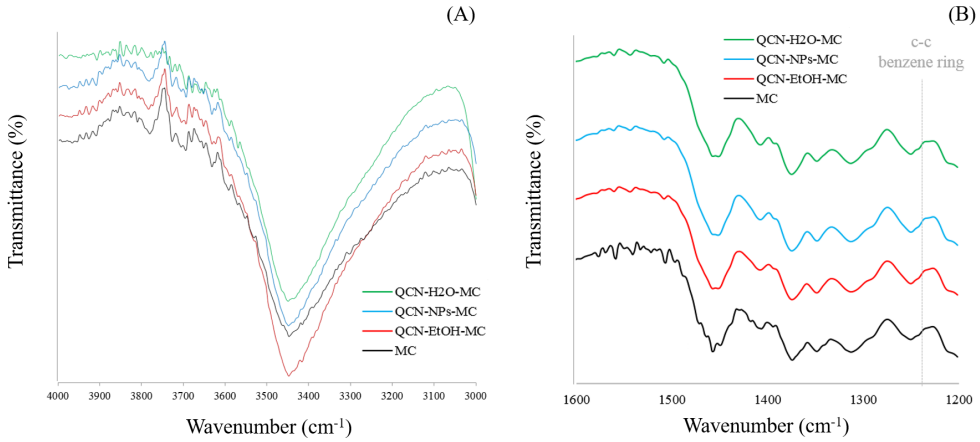

Fig. 9 Fourier transform infrared spectroscopy spectra of methylcellulose (MC) and 0.5 wt% quercetin (QC)-EtOH-MC film, QC-nanoparticles-MC film and QC-H_2O-MC film in the regions: (A) 4000–3000 cm^{-1}; (B)1600–1200 cm^{-1}

and QC-NPs-MC film were 6.74 cm^{-1}, 8.58 cm^{-1} and 10.60 cm^{-1}, respectively. These substantiated the hydrogen bonding interactions, in connection with the existence of hydrogen bonding between MC−MC, MC−PEG400 and MC−QC molecules. The countless hydrogen bonds between the MC chains were conducive to many MC−MC interactions and therefore contributed to the cohesiveness and flexibility of the unplasticized MC film. PEG400 is known as a good plasticizer for MC films, since it lowers the tensile strength (Debeaufort and Voilley, 1997). Generally, when either PEG400 or QC is impregnated in the MC network, there is potential for hydrogen bonding between MC−MC and MC−PEG or MC−QC. Hence, direct interactions between and the adjacency of MC chains are decreased, partially due to hydrogen bond formation with either PEG400 or QC. The results indicated there were no significant differences in BSD among the MC films fabricated using different ethanol concentrations with or without PEG400 (Turhan et al., 2001). This suggested that neither ethanol nor its concentration influenced symmetry distortion. This was an expected consequence since ethanol exclusively promoted a shorter drying time because of its low boiling point (78°C) and so it did not persist in the films after drying. Consequently, it did not firmly amend the polymeric structure of MC. Similar results were reported by Debeaufort and Voilley (1997), who stated that ethanol did not alter the structure and thermal properties of MC. Because of the very low concentrations of QC-EtOH, QC-NPs and QC-H_2O incorporated in the MC films, the characteristic peaks of QC could not be discerned in the spectra of the QC-EtOH-MC film, QC-NPs-MC film or QC-H_2O-MC film.

Total phenolic content and antioxidant activities of films

As revealed in Table 4, the results from all assays (TPC, DPPH, ABTS and FRAP) showed that the TPC and AO activities tended to significantly increase with increasing bioactive concentration in the film formulation. However, for all concentrations of BHT-incorporated cellulose-based films, the TPC and FRAP values were not measurable because of the lack of a dose-response. This was in accord with the study by Saelo et al. (2016). Both the TPC and FRAP values of the QC-NPs-MC film were high and greater than those of the QC-EtOH-MC film and QC-H_2O-MC film because of the smaller particle size in the former. According to the concentration effect, the TPC was well correlated with FRAP (r = 0.990) and much less correlated with DPPH (r = 0.836), as shown in Table 5.

As each assay used different conditions that had tier specific benefits and drawbacks, a single assay is not suitable to represent the effectiveness of antioxidants, unless the conditions are similar (Frankel and Meyer, 2000). Consequently, it is essential to carry out more than one assay to investigate the various mechanisms of AO activity. Table 5 indicates that there was a significant positive correlation between DPPH radical scavenging and ABTS radical cation scavenging (due to hydrogen atoms and electron transfer). In addition, the FRAP and TPC assays measured the ability of QC to reduce metal ions through electron transfer. This finding was in accordance with Song et al. (2010). Because the coefficient of determination was quite high, either the DPPH or ABTS assay could be chosen to evaluate the AO effectiveness of QC.

Table 4 Total phenolic content and antioxidant activities of methylcellulose films containing 3-tert-Butyl-4-hydroxyanisole (BHA), 3,5-ditert-butyl-4-hydroxytoluene (BHT), quercetin (QC)-EtOH, QC-nanoparticles (NPs) and QC-H_2O

Antioxidant	Concentration (% weight per weight)	TPC (μg GAE/mL)	DPPH scavenging (%)	ABTS scavenging (%)	FRAP (TE μM/mL)
BHA	0.10	1.12±0.23^{n}	11.59±1.72^{n}	11.18±4.30^{n}	12.93±2.35^{n}
	0.20	1.79±0.16^{mn}	21.93±2.98^{l}	20.53±5.65^{m}	24.42±3.14^{lm}
	0.30	2.49±0.28^{m}	36.11±2.06^{i}	34.47±5.54^{k}	40.76±1.20^{k}
	0.40	3.45±0.52^{l}	42.37±6.33^{h}	40.01±10.53^{i}	50.42±5.92^{j}
	0.50	4.23±0.58^{k}	44.56±5.84^{g}	46.66±5.02^{i}	58.50±6.78^{j}
BHT	0.10	ND	6.45±0.67^{p}	1.47±0.14^{q}	ND
	0.20	ND	8.10±0.23^{o}	2.20±0.40^{pq}	ND
	0.30	ND	8.84±0.20^{o}	3.40±0.34^{pq}	ND
	0.40	ND	9.44±0.28^{o}	4.11±0.22^{op}	ND
	0.50	ND	11.34±0.87^{n}	5.89±0.56^{o}	ND
QC-EtOH	0.10	4.48±0.40^{k}	28.09±1.95^{k}	23.42±4.37^{l}	29.90±1.81^{l}
	0.20	10.07±0.56^{i}	49.89±9.02^{e}	45.32±10.01^{h}	60.33±8.95^{i}
	0.30	14.33±0.95^{g}	66.31±2.84^{c}	68.94±4.91^{f}	109.61±2.88^{g}
	0.40	22.93±0.93^{c}	72.86±1.87^{b}	76.31±5.28^{e}	152.58±12.36^{d}
	0.50	26.30±1.69^{b}	74.42±1.60^{ab}	88.20±2.50^{b}	173.83±7.83^{c}
QC-NPs	0.10	5.86±0.45^{j}	37.04±2.21^{i}	31.16±4.59^{k}	42.42±3.16^{k}
	0.20	10.67±1.01^{i}	61.58±6.31^{d}	57.77±7.05^{g}	84.58±10.72^{h}
	0.30	16.98±0.63^{f}	68.33±1.92^{c}	81.08±3.66^{cd}	145.89±8.60^{e}
	0.40	23.63±1.51^{c}	72.46±1.99^{b}	83.13±7.29^{b}	182.75±17.92^{b}
	0.50	33.20±1.15^{a}	75.22±0.84^{a}	95.72±1.25^{a}	292.99±9.86^{a}
QC-H_2O	0.10	2.32±0.14^{m}	15.99±1.18^{m}	16.85±3.20^{m}	20.89±1.42^{m}
	0.20	6.59±0.64^{j}	35.32±3.99^{j}	32.46±5.12^{j}	42.98±3.41^{k}
	0.30	11.65±0.71^{h}	49.73±0.71^{g}	53.36±5.48^{h}	80.08±6.39^{h}
	0.40	17.89±0.53^{e}	55.55±1.33^{f}	58.68±5.20^{d}	123.34±13.67^{f}
	0.50	20.84±1.32^{d}	60.39±1.69^{d}	71.22±5.46^{c}	142.07±2.53^{e}

TPC = total phenolic content; DPPH = 2,2-diphenyl-1-picrylhydrazyl; ABTS = 2,2'-azino-bis (3-ethylbenzthiazoline-6-sulphonic acid); FRAP = ferric reducing antioxidant power; GAE = gallic acid equivalent; TE = Trolox equivalents; ND = values are not quantifiable due to lack of dose-response
Values (mean ± SD) within the same column superscripted with different lowercase letters are significantly ($p < 0.05$) different.

Table 5 Pearson correlation coefficients among total phenolic content (TPC) and three antioxidant activities of quercetin nanoparticles incorporated in methylcellulose films

	DPPH	ABTS	FRAP	TPC
DPPH	1.000			
ABTS	0.950	1.000		
FRAP	0.823	0.896	1.000	
TPC	0.836	0.908	0.990	1.000

DPPH = 2,2-diphenyl-1-picrylhydrazyl; ABTS = 2,2'-azino-bis (3-ethylbenzthiazoline-6-sulphonic acid); FRAP = ferric reducing antioxidant power.
All correlation coefficients are highly significant ($p < 0.01$).

In this research, QC-NPs were favorably prepared in a single step using the RESOLV process. QC-NPs stabilized in pluronic F127 were well-dispersed in the nanosuspension and were spherical, with individual NPs having an average size of approximately 60 nm and 500 nm based on TEM and DLS, respectively. Both the QC-NPs and QC-EtOH had higher AO capacities to scavenge DPPH, ABTS and reduce the ferric complex to ferrous form than those of QC-H_2O, BHA and BHT. The impregnation of QC into MC films was verified based on the FTIR spectra. This study also demonstrated that QC can be incorporated as nanoparticles into MC films. The QC-NPs incorporated into MC films showed potent AO activities and offered considerable UV protection. This work demonstrated that QC-NPs substantially improved the bioactive properties of

QC. Therefore, it is recommended that QC-NPs incorporated into MC films and coatings may be used as bioactive food packaging materials, contributing to food preservation and prolonging the shelf life of edible food items.

Conflict of Interest

The authors declare that there are no conflicts of interest.

Acknowledgements

This research was supported in part by the Graduate Program Scholarship from the Graduate School, Kasetsart University, Bangkok, Thailand and by funds for the promotion of research at the Center of Advanced Studies for Agriculture and Food (CASAF) and the Center for Advanced Studies in Nanotechnology and Its Applications in Chemical, Food and Agricultural Industries (CASNACFAI), Kasetsart University. The corresponding author expresses his thanks and appreciation for all these contributions. Mr Suwit Kongsakorn, Department of Packaging and Materials Technology, Faculty of Agro-Industry, Kasetsart University, prepared the QC nanoparticles.

References

Afia, L., Larouj, M., Salghi, R., Jodeh, S., Zougagh, M., Hasan, A.R., Lgaz, H. 2016. Experimental and theoretical evaluation of quercetin as a novel and eco-friendly corrosion inhibitor for C38 steel in hydrochloric medium. Der Pharma Chem. 8: 166–179.

Ahmed, S., Ikram, S. 2016. Chitosan and gelatin based biodegradable packaging films with UV-light protection. J. Photochem. Photobiol. B, Biol. 163: 115–124. doi.org/10.1016/j.jphotobiol.2016.08.023

Alam, M.N., Bristi, N.J., Rafiquzzaman, M. 2013. Review on *in vivo* and *in vitro* methods evaluation of antioxidant activity. Saudi Pharm. J. 21: 143–152. doi.org/10.1016/j.jsps.2012.05.002

Andrade-Filho, T., Ribeiro, T.C.S., Del Nero, J. 2009. The UV-vis absorption spectrum of the flavonol quercetin in methanolic solution: A theoretical investigation. Eur. Phys. J.E 29: 253–259. doi.org/10.1140/epje/i2009-10485-7

Bekbölet, M. 1990. Light effects on food. J. Food Prot. 53: 430–440. doi.org/10.4315/0362-028X-53.5.430

Bhattacharjee, S. 2016. DLS and zeta potential - What they are and what they are not? J. Control. Release. 235: 337–351. doi.org/10.1016/j.jconrel.2016.06.017

Boots, A.W., Haenen, G.R., Bast, A. 2008. Health effects of quercetin: From antioxidant to nutraceutical. Eur. J. Pharmacol. 585: 325–337. doi.org/10.1016/j.ejphar.2008.03.008

Bukhari, S.B., Memon, S., Mahroof-Tahir, M., Bhanger, M.I. 2008. Synthesis, characterization and investigation of antioxidant activity of cobalt-quercetin complex. J. Mol. Struct. 892: 39–46. doi.org/10.1016/j.molstruc.2008.04.050

Bourtoom, T. 2008. Edible films and coatings: Characteristics and properties. Int. Food Res. J. 15: 237–248.

Cangelosi, F., Shaw, M.T. 1983. A review of hydrogen bonding in solid polymers: Structural relationships, analysis, and importance. Polym. Plast. Technol. Eng. 21: 13–98. doi.org/10.1080/03602558308070020

Chafer, A., Fornari, T., Berna, A., Stateva, R.P. 2004. Solubility of quercetin in supercritical CO_2 + ethanol as a modifier: Measurements and thermodynamic modelling. J. Supercrit. Fluids. 32: 89–96. doi.org/10.1016/j.supflu.2004.02.005

Choe, E., Min, D.B. 2009. Mechanisms of antioxidants in the oxidation of foods. Compr. Rev. Food Sci. Food Saf. 8: 345–358. doi.org/10.1111/j.1541-4337.2009.00085.x

Cornard, J.P., Merlin, J.C., Boudet, A.C., Vrielynck, L. 1997. Structural study of quercetin by vibrational and electronic spectroscopies combined with semiempirical calculations. Biospectroscopy 3: 183–193. doi.org/10.1002/(SICI)1520-6343(1997)3:3<183::AID-BSPY2>3.0.CO;2-7

Debeaufort, F., Voilley, A. 1997. Methylcellulose-based edible films and coatings. 2. Mechanical and thermal properties as a function of plasticizer content. J. Agric. Food Chem. 45: 685–689.

Dehghan, G., Khoshkam, Z. 2012. Tin(II)-quercetin complex: Synthesis, spectral characterisation and antioxidant activity. Food Chem. 131: 422–426. doi.org/10.1016/j.foodchem.2011.08.074

de Moraes Crizel, T., de Oliveira Rios, A., Alves, V.D., Bandarra, N., Moldão-Martins, M., Hickmann Flôres, S. 2018. Active food packaging prepared with chitosan and olive pomace. Food Hydrocoll. 74: 139–150. doi.org/10.1016/j.foodhyd.2017.08.007

de Paz, E., Martín, Á., Every, H., Cocero, M.J. 2015. Production of water-soluble quercetin formulations by antisolvent precipitation and supercritical drying. J. Supercrit. Fluids. 104: 281–290. doi.org/10.1016/j.supflu.2015.07.006

Dueñas, M., González-Manzano, S., González-Paramás, A., Santos-Buelga, C. 2010. Antioxidant evaluation of O-methylated metabolites of catechin, epicatechin and quercetin. J. Pharm. Biomed. Anal. 51: 443–449. doi.org/10.1016/j.jpba.2009.04.007

Ezati, P., Rhim, J.-W. 2021. Fabrication of quercetin-loaded biopolymer films as functional packaging materials. ACS Appl. Polym. Mater. 3: 2131–2137. doi.org/10.1021/acsapm.1c00177

Fernández-Ponce, M.T., Masmoudi, Y., Djerafi, R., Casas, L., Mantell, C., de la Ossa, E.M., Badens, E. 2014. Particle design applied to quercetin using supercritical anti-solvent techniques. J. Supercrit. Fluids. 105: 119–127. doi.org/10.1016/j.supflu.2015.04.014

Fissan, H., Ristig, S., Kaminski, H., Asbach, C., Epple, M. 2014. Comparison of different characterization methods for nanoparticle dispersions before and after aerosolization. Anal. Methods 6: 7324–7334. doi.org/10.1039/C4AY01203H

Foti, M.C., Daquino, C., Dilabio, G.A., Ingold, K.U. 2011. Kinetics of the oxidation of quercetin by 2,2-diphenyl-1-picrylhydrazyl (dpph•). Org. Lett. 13: 4826–4829. doi.org/10.1021/ol2019086

Fraile, M., Buratto, R., Gómez, B., Martín, Á., Cocero, M.J. 2014. Enhanced delivery of quercetin by encapsulation in poloxamers by supercritical antisolvent process. Ind. Eng. Chem. Res. 53: 4318–4327. doi.org/10.1021/ie5001136

Frankel, E.N., Meyer, A.S. 2000. The problems of using one-dimensional methods to evaluate multifunctional food and biological antioxidants. J. Sci. Food Agric. 80: 1925–1941. doi.org/10.1002/1097-0010(200010)80:13<1925::AID-JSFA714>3.0.CO;2-4

Ganiari, S., Choulitoudi, E., Oreopoulou, V. 2017. Edible and active films and coatings as carrier of natural antioxidant for lipid food. Trends Food Sci. Technol. 68: 70–82. doi.org/10.1016/j.tifs.2017.08.009

Gasti, T., Dixit, S., D'souza, O.J., Hiremani, V.D., Vootla, S.K., Masti, S.P., Chougale, R.B.,

Malabadi, R.B. 2021. Smart biodegradable films based on chitosan/methylcellulose containing *Phyllanthus reticulatus* anthocyanin for monitoring the freshness of fish fillet. Int. J. Biol. Macromol. 187: 451–461. doi.org/10.1016/j.ijbiomac.2021.07.128

Gómez-Estaca, J., López-de-Dicastillo, C., Hernández-Muñoz, P., Catalá, R., Gavara, R. 2014. Advance in antioxidant active food packaging. Trends Food Sci. Technol. 35: 42–51. doi.org/10.1016/j.tifs.2013.10.008

Gordon, M.H. 1990. The mechanism of antioxidant action in vitro. In: Hudson B.J.F. (Ed.). Food Antioxidants. Elsevier. New York, NY, USA, pp. 1–18.

Goudar, N., Vanjeri, V.N., Kasai, D., Gouripur, G., Malabadi, R.B., Masti, S.P., Chougale, R.B. 2021. ZnO NPs doped PVA/*Spathodea campanulata* thin films for food packaging. J. Polym. Environ. 29: 2797–2812. doi.org/10.1007/s10924-021-02070-0

Goupy, P., Dufour, C., Loonis, M., Dangles, O. 2003. Quantitative kinetic analysis of hydrogen transfer reactions from dietary polyphenols to the DPPH radical. J. Agric. Food Chem. 51: 615–622. doi.org/10.1021/jf025938l

Griffin, S.P., Bhagooli, R. 2004. Measuring antioxidant potential in corals using the FRAP assay. J. Exp. Mar. Biol. Ecol. 302: 201–211. doi.org/10.1016/j.jembe.2003.10.008

Hannon, J.C., Kerry, J., Cruz-Romero, M., Morris, M., Cummins, E. 2015. Advances and challenges for the use of engineered nanoparticles in food contact materials. Trends Food Sci. Technol. 43: 43−62. doi.org/10.1016/j.tifs.2015.01.008

Hatahet, T., Morille, M., Hommoss, A., Dorandeu, C., Müller, R.H., Bégu, S. 2016. Dermal quercetin smartCrystals®: Formulation development, antioxidant activity and cellular safety. Eur. J. Pharm. Biopharm. 102: 51–63. doi.org/10.1016/j.ejpb.2016.03.004

Hu, D., Zhang, Z., Liu, M., Lin, J., Chen, X., Ma, W. 2019. Multifunctional UV-shielding nanocellulose films modified with halloysite nanotubes-zinc oxide nanohybrid. Cellulose 27: 401–413. doi.org/10.1007/s10570-019-02796-0

Jiang, J., Oberdörster, G., Biswas, P. 2009. Characterization of size, surface charge, and agglomeration state of nanoparticle dispersions for toxicological studies. J. Nanopart. Res. 11: 77–89. doi.org/10.1007/s11051-008-9446-4

Johnson, R.K., Zink-Sharp, A., Renneckar, S.H., Glasser, W.G. 2009. A new bio-based nanocomposite: fibrillated TEMPO-oxidized celluloses in hydroxypropylcellulose matrix. Cellulose 16: 227–238. doi.org/10.1007/s10570-008-9269-6

Kakran, M., Sahoo, N.G., Li, L., Judeh, Z. 2012. Fabrication of quercetin nanoparticles by anti-solvent precipitation method for enhanced dissolution. Powder Technol.223: 59–64. doi.org/10.1016/j.powtec.2011.08.021

Kester, J.J., Fennema, O.R. 1986. Edible films and coatings: A review. Food Technol.40: 47–59.

Khan, R.A., Salmieri, S., Dussault, D., Uribe-Calderon, J., Kamal, M.R., Safrany, A., Lacroix, M. 2010. Production and properties of nanocellulose-reinforced methylcellulose-based biodegradable films. J. Agric. Food Chem. 58: 7878–7885. doi.org/10.1021/jf1006853

Kitak, T., Dumičić, A., Planinšek, O., Šibanc, R., Srčič, S. 2015. Determination of solubility parameters of ibuprofen and ibuprofen lysinate. Molecules 20: 21549−21568. doi.org/10.3390/molecules201219777

Kumar, D.V., Verma, P.R.P., Singh, S.K. 2016. Morphological and in vitro antibacterial efficacy of quercetin loaded nanoparticles against food-borne microorganisms. LWT. 66: 638–650. doi.org/10.1016/j.lwt.2015.11.004

Kumari, A., Yadav, S.K., Pakade, Y.B., Singh, B., Yadav, S.C. 2010. Development of biodegradable nanoparticles for delivery of quercetin. Colloids Surf. B. 80: 184–192. doi.org/10.1016/j.colsurfb.2010.06.002

Lee, L.S., Choi, E.J., Kim, C.H., et al. 2016. Contribution of flavonoids to the antioxidant properties of common and tartary buckwheat. J. Cereal Sci. 68: 181–186. doi.org/10.1016/j.jcs.2015.07.005

Lizundia, E., Ruiz-Rubio, L., Vilas, J.L., León, L.M. 2016. Poly(l-lactide)/ZnO nanocomposites as efficient UV-shielding coatings for packaging applications. J. Appl. Polym. Sci. 133: 42426. doi.org/10.1002/app.42426

Lopez-Rubio, A., Gavara, R., Lagaron, J.M. 2006. Bioactive packaging: Turning foods into healthier foods through biomaterials. Trends Food Sci. Technol. 17: 567−575. doi.org/10.1016/j.tifs.2006.04.012

Lu, L.J., Lu, L.X. 2018. Preparation and properties of quercetin-incorporated high density polyethylene/low density polyethylene antioxidant multilayer film. Packag. Technol. Sci. 31: 433–439. doi.org/10.1002/pts.2371

Maalik, A., Khan, F.A., Mumtaz, A., Mehmood, A., Azhar, S., Atif, M., Karim, S., Altaf, Y.,

Tariq, I. 2014. Pharmacological applications of quercetin and its derivatives: A short review. Trop. J. Pharm. Res. 13: 1561–1566. doi.org/10.4314/tjpr.v13i9.26

Materska, M. 2008. Quercetin and its derivatives: Chemical structure and bioactivity − A review. Pol. J. Food Nutr. Sci. 58: 407−413.

Montes, A., Pereyra, C., De La Ossa, E.J.M. 2015. Screening design of experiment applied to the supercritical antisolvent precipitation of quercetin. J. Supercrit. Fluids. 104: 10–18. doi.org/10.1016/j.supflu.2015.05.019

Pabisch, S., Feichtenschlager, B., Kickelbick, G., Peterlik, H. 2012. Effect of interparticle interactions on size determination of zirconia and silica based systems - A comparison of SAXS, DLS, BET, XRD and TEM. Chem. Phys. Lett. 521: 39–46. doi.org/10.1016/j.cplett.2011.11.049

Park, S., Jeon, Y., Han, T., Kim, S., Gwon, Y., Kim, J. 2020. Nanoscale manufacturing as an enabling strategy for the design of smart food packaging systems. Food Packag. Shelf Life. 26: 100570. doi.org/10.1016/j.fpsl.2020.100570

Pinelo, M., Manzocco, L., Nuñez, M.J., Nicoli, M.C. 2004. Solvent effect on quercetin antioxidant capacity. Food Chem. 88: 201–207. doi.org/10.1016/j.foodchem.2004.01.034

Pungor, E. 1995. A Practical Guide to Instrumental Analysis, 1st ed. CRC Press Inc. Boca Raton, FL, USA.

Ravichandran, R., Rajendran, M., Devapiriam, D. 2014. Antioxidant study of quercetin and their metal complex and determination of stability constant by spectrophotometry method. Food Chem. 146: 472–478. doi.org/10.1016/j.foodchem.2013.09.080

Rimdusit, S., Somsaeng, K., Kewsuwan, P., Jubsilp, C., Tiptipakorn, S. 2012. Comparison of gamma radiation crosslinking and chemical crosslinking on properties of methylcellulose hydrogel. Eng. J. 16: 16–28. doi.org/10.4186/ej.2012.16.4.15

Saelo, S., Assatarakul, K., Sane, A., Suppakul, P. 2016. Fabrication of novel bioactive cellulose-based films derived from caffeic acid phenethyl ester-loaded nanoparticles via a rapid expansion process: RESOLV. J. Agric. Food Chem. 64: 6694–6707. doi.org/10.1021/acs.jafc.6b02197

Sánchez-Rangel, J.C., Benavides, J., Heredia, J.B., Cisneros-Zevallos, L., Jacobo-Velázquez, D.A. 2013. The Folin-Ciocalteu assay revisited: Improvement of its specificity for total phenolic content determination. Anal. Methods 5: 5990–5999. doi.org/10.1039/C3AY41125G

Sanches-Silva, A., Costa, D., Albuquerque, T.G., Buonocore, G.G., Ramos, F., Castilho, M.C., Machado, A.V., Costa, H.S. 2014. Trends in the use of natural antioxidants in active food packaging: A review. Food Addit. Contam. Part A. 31: 374–395. doi.org/10.1080/19440049.2013.879215

Sane, A., Thies, M.C. 2005. The formation of fluorinated tetraphenylporphyrin nanoparticles via rapid expansion processes: RESS vs RESOLV. J. Phys. Chem. B 109: 19688–19695. doi.org/10.1021/jp0581072

Shankar, S., Rhim, J.W. 2019. Effect of types of zinc oxide nanoparticles on structural, mechanical and antibacterial properties of poly(lactide)/poly(butylene adipate-co-terephthalate) composite films. Food Packag. Shelf Life. 21: 100327. doi.org/10.1016/j.fpsl.2019.100327

Singleton, V.L., Rossi, J.A. 1965. Colorimetry of total phenolics with phosphomolybdic-phosphotungstic acid reagents. Am. J. Enol. Vitic. 16: 144–158.

Siripatrawan, U., Harte, B.R. 2010. Physical properties and antioxidant activity of an active film from chitosan incorporated with green tea extract. Food Hydrocoll. 24: 770–775. doi.org/10.1016/j.foodhyd.2010.04.003

Sisa, M., Bonnet, S.L., Ferreira, D., Van der Westhuizen, J.H. 2010. Photochemistry of flavonoids. Molecules 15: 5196–5245. doi.org/10.3390/molecules15085196

Song, F.L., Gan, R.Y., Zhang, Y., Xiao, Q., Kuang, L., Li, H.B. 2010. Total phenolic contents and antioxidant capacities of selected Chinese medicinal plants. Int. J. Mol. Sci. 11: 2362–2372. doi.org/10.3390/ijms11062362

Songtipya, L., Sane, A. 2013. Effect of concentration and degree of saturation on co-precipitation of catechin and poly(L-lactide) by the RESOLV process. J. Supercrit. Fluids. 75: 72–80. doi.org/10.1016/j.supflu.2012.12.024

Songtipya, L., Thies, M.C., Sane, A. 2016. Effect of rapid expansion of subcritical solutions processing conditions on loading capacity of tetrahydrocurcumin encapsulated in poly(L-lactide) particles. J. Supercrit. Fluids. 113: 119–127. doi.org/10.1016/j.supflu.2016.03.020

Sonkaew, P., Sane, A., Suppakul, P. 2012. Antioxidant activities of curcumin and ascorbyl dipalmitate nanoparticles and their activities after incorporation into cellulose-based packaging films. J. Agric. Food Chem. 60: 5388–5398. doi.org/10.1021/jf301311g

Souza, M.P., Vaz, A.F.M., Silva, H.D., Cerqueira, M.A., Vicente, A.A., Carneiro-da-Cunha, M.G. 2015. Development and characterization of an active chitosan-based film containing quercetin. Food Bioprocess Tech. 8: 2183–2191. doi.org/10.1007/s11947-015-1580-2

Suppakul, P., Jutakorn, K., Bangchokedee, Y. 2010. Efficacy of cellulose-based coating on enhancing the shelf life of fresh eggs. J. Food Eng. 98: 207–213. doi.org/10.1016/j.jfoodeng.2009.12.027

Tavassoli, M., Sani, M.A., Khezerlou, A., Ehsani, A., McClements, D.J. 2021. Multifunctional nanocomposite active packaging materials: Immobilization of quercetin, lactoferrin, and chitosan nanofiber particles in gelatin films. Food Hydrocoll. 118: 106747. doi.org/10.1016/j.foodhyd.2021.106747

Tavera-Quiroz, M.J., Urriza, M., Pinotti, A., Bertola, N. 2012. Plasticized methylcellulose coating for reducing oil uptake in potato chips. J. Sci. Food Agric. 92: 1346–1353. doi.org/10.1002/jsfa.4704

Thaipong, K., Boonprakob, U., Crosby, K., Cisneros-Zevallos, L., Hawkins Byrne, D. 2006. Comparison of ABTS, DPPH, FRAP, and ORAC assays for estimating antioxidant activity from guava fruit extracts. J. Food Compos. Anal. 19: 669–675. doi.org/10.1016/j.jfca.2006.01.003

Turhan, K.N., Sahbaz, F., Güner, A. 2001. A spectrophotometric study of hydrogen bonding in methylcellulose-based edible films plasticized by polyethylene glycol. J. Food Sci. 66: 59–62. doi.org/10.1111/j.1365-2621.2001.tb15581.x

Türk, M. 2009. Manufacture of submicron drug particles with enhanced dissolution behaviour by rapid expansion processes. J. Supercrit. Fluids. 47: 537–545. doi.org/10.1016/j.supflu.2008.09.008

Viera, R.G.P., Filho, G.R., de Assunção, R.M.N., da Carla, C., Vieira, J.G., de Oliveira, G.S. 2007. Synthesis and characterization of methylcellulose from sugar cane bagasse cellulose. Carbohydr. Polym. 67: 182–189. doi.org/10.1590/S0104-14282012005000011

Vilera, C., Pinto, R.J.B., Coelho, J., Domingues, M.R.M., Daina, S., Sadocco, P., Santos, S.A.O., Freire, C.S.R. 2017. Bioactive chitosan/ellagic acid films with UV-light protection for active food packaging. Food Hydrocoll. 73: 120–128. doi.org/10.1016/j.foodhyd.2017.06.037

Vinogradov, S.N., Linnell, R.H. 1971. Hydrogen bonding. Van Nostrand Reinhold. New York, NY, USA.

Wu, T., Yen, F., Liang, L., Tsai, T., Lin, C., Cham, T. 2008. Preparation, physicochemical characterization, and antioxidant effects of quercetin nanoparticles. Int. J. Pharm. 346: 160–168. doi.org/10.1016/j.ijpharm.2007.06.036

Xu, D., Hu, M.J., Wang, Y.Q., Cui, Y.L. 2019. Antioxidant activities of quercetin and its complexes for medicinal application. Molecules 24: 1123. doi.org/10.3390/molecules24061123

Zheng, Y.Z., Deng, G., Liang, Q., Chen, D.F., Guo, R., Lai, R.C. 2017. Antioxidant activity of quercetin and its glucosides from propolis: A theoretical study. Sci. Rep. 7: 7543. doi.org/10.1038/s41598-017-08024-8